

# Daytime urban breeze circulation and its interaction with convective cells

Young-Hee Ryu, Jong-Jin Baik\* and Ji-Young Han

*School of Earth and Environmental Sciences, Seoul National University, Seoul, South Korea*

\*Correspondence to: J.-J. Baik, School of Earth and Environmental Sciences, Seoul National University, Seoul 151-742, South Korea. E-mail: jjbaik@snu.ac.kr

The structure and evolution of daytime urban breeze circulation (UBC) and its interaction with convective cells in two dimensions are examined through high-resolution numerical model simulation. The UBC is the thermally forced, solenoidal circulation that results from the difference in surface energy balance between the urban and rural areas. As the temperature excess in the urban area increases, the UBC becomes larger and stronger with time and the two urban-breeze fronts (the leading edges of the UBC) that initially form at the urban-rural boundaries in the morning move toward the urban centre. Meanwhile, due to strong surface heating in the daytime, a number of convective cells form in both the rural and urban areas and the different characteristics between rural and urban convective cells are identified. The aspect ratio of the urban cells is smaller than that of the rural cells, which is partly attributed to the deeper urban boundary layer. The cell updrafts originating from the urban area are stronger, warmer and drier than those from the rural area. As the UBC develops, the convective cells that form in the rural area are advected toward the urban area by the UBC. Under the influence of the UBC, the cell updrafts originating from the rural area weaken and the water vapour mixing ratio in the updrafts decreases. As the cell updrafts originating from both the rural and urban areas merge with the urban-breeze front, the front intensity increases and the water vapour mixing ratio at the front is modulated. Copyright © 2012 Royal Meteorological Society

**Key Words:** urban heat island; urban boundary layer; urban breeze circulation; convective cells

*Received 12 December 2011; Revised 24 April 2012; Accepted 26 April 2012; Published online in Wiley Online Library 13 June 2012*

*Citation:* Ryu Y-H, Baik J-J, Han J-Y. 2013. Daytime urban breeze circulation and its interaction with convective cells. *Q. J. R. Meteorol. Soc.* **139**: 401–413. DOI:10.1002/qj.1973

## 1. Introduction

The distinctive surface features of urban areas, such as paved surfaces, low- and high-rise buildings and the scarcity of vegetation, together with anthropogenic heat significantly alter the surface energy balance (SEB) in urban areas. One of the most distinctive features of the urban SEB is the almost exclusive partitioning of the available net radiation into sensible heat flux (including storage heat flux) in the daytime, which is mainly attributed to the reduction of daytime evapotranspiration resulting from the scarcity of pervious surfaces in urban areas (Oke, 1982, 1988).

The sensible heat flux in urban areas can remain positive even in the night-time due to the large storage heat flux, which is not likely to occur in rural areas. The differential heating and cooling associated with the difference in the SEB between urban and rural areas leads to the well-known anthropogenic climate modification, the urban heat island (UHI). The observed UHI intensity is generally 1–2 K in the daytime (e.g. Kim and Baik, 2002; Giridharan *et al.*, 2007; Hidalgo *et al.*, 2008a).

The horizontal temperature gradient between urban and rural areas associated with the UHI induces a horizontal pressure gradient. This induces an urban breeze circulation

(UBC) that is characterized by inward flow toward the urban area (a city) in the lower boundary layer and by outward flow toward the surroundings in the upper boundary layer. Warmer air rises over the city, and cooler air is drawn into the city from the surroundings (Hidalgo *et al.*, 2010).

The UBC, also called the UHI circulation, has been observed from aircraft measurements over St Louis, USA (Wong and Dirks, 1978) and over Toulouse, France (Hidalgo *et al.*, 2008a), and it has also been investigated by using numerical models that include SEB models (Avissar, 1996; Lemonsu and Masson, 2002; Kusaka and Kimura, 2004; Hidalgo *et al.*, 2008b). From the aircraft measurements in the St Louis metropolitan area, Dirks (1974) found a positive potential temperature anomaly of up to 2 K and a negative specific humidity anomaly of up to  $2.5 \text{ g kg}^{-1}$  in the daytime boundary layer under light wind conditions. Hidalgo *et al.* (2008a) observed similar features in Toulouse and documented a positive potential temperature anomaly of  $\sim 1 \text{ K}$  and a negative specific humidity anomaly of  $\sim 0.3 \text{ g kg}^{-1}$  in the daytime boundary layer. They also documented that in the afternoon the intensity of the UBC estimated from wind anomalies is  $1\text{--}2 \text{ m s}^{-1}$  in the horizontal direction and that the horizontal extent of the UBC in the afternoon is two to three times larger than the size of the city. In numerical modelling studies, the larger sensible heat flux by  $100\text{--}400 \text{ W m}^{-2}$  and the higher potential temperature by  $\sim 1 \text{ K}$  in urban areas in the afternoon under light wind conditions were commonly reported (Avissar, 1996; Lemonsu and Masson, 2002; Kusaka and Kimura, 2004; Hidalgo *et al.*, 2008b). The UBCs exhibit the strongest intensity in the late afternoon with  $2\text{--}7 \text{ m s}^{-1}$  in the horizontal and  $\sim 1 \text{ m s}^{-1}$  in the vertical (Lemonsu and Masson, 2002; Hidalgo *et al.*, 2008b). In addition, the higher urban boundary layer by  $\sim 300 \text{ m}$  was reported in both observational and modelling studies (Dirks, 1974; Kusaka and Kimura, 2004; Hidalgo *et al.*, 2008b).

There are a number of studies that have investigated UBCs by conducting laboratory experiments (e.g. Noto, 1996; Lu *et al.*, 1997a,b), by using numerical models (e.g. Delage and Taylor, 1970; Baik *et al.*, 2001) and by using analytic models (e.g. Vukovich, 1971; Baik, 1992; Baik and Chun, 1997), but those studies did not consider surface energy budget and prescribed a heat island. Moreover, those studies mostly considered stable conditions. Stable conditions are not conducive to vertical motion over the city (Shreffler, 1978). Despite the substantial studies of UBCs, the structure and evolution of the UBC that develops in a convective boundary layer (CBL) in response to the difference in urban and rural SEBs are not well understood. Furthermore, like other mesoscale circulations such as sea breeze, river breeze and dryline circulations, the UBC can interact with other organized convection in the CBL.

Cellular convection, which takes the form of either two-dimensional rolls (also known as horizontal convective rolls) or three-dimensional cellular cells, is one of the common forms of atmospheric boundary layer convection (Tian *et al.*, 2003) and has been investigated extensively by numerous researchers. In this study, these types of convection are simply referred to as convective cells. Although UBC and convective cells have been investigated individually, the interaction between the UBC and convective cells has not yet been demonstrated, to the authors' knowledge. Miao *et al.* (2009) performed real-data simulations to examine UHI characteristics and related phenomena in

Beijing, China. They showed that horizontal convective rolls usually occur in the urban area and cellular cells occur in the rural area. However, they did not study a UBC and its interaction with convective cells. The objective of this study is to investigate the structure and evolution of a daytime UBC and its interaction with convective cells that form in both rural and urban areas.

Previous studies on the interaction between convective cells and other mesoscale circulations, such as sea breeze (Atkins *et al.*, 1995; Dailey and Fovell, 1999; Ogawa *et al.*, 2003), river breeze (Rao *et al.*, 1999) and dryline (Atkins *et al.*, 1998; Peckham *et al.*, 2004; Wakimoto *et al.*, 2006; Xue and Martin, 2006) circulations, have emphasized that convective cells significantly modulate the frontal structures of the sea breeze, river breeze and dryline, thus leading to the horizontal variability of the frontal structures. For example, horizontal convective rolls create vertical velocity maxima at the points where they intersect with the dryline, which plays a key role for initiating clouds at these intersection points (Atkins *et al.*, 1998). In a similar way, it is expected that the interaction between a UBC and convective cells can play an important role in modulating urban-breeze frontal structure and convective activity.

In section 2, the experimental design is described. Results are presented and discussed in section 3. A summary and conclusions are provided in section 4.

## 2. Experimental design

The advanced research weather research and forecasting (WRF) model version 3.2 (Skamarock *et al.*, 2008) is employed in this study. Physical parametrization options used are the Dudhia shortwave radiation scheme (Dudhia, 1989), the rapid radiative transfer model (RRTM) longwave radiation scheme (Mlawer *et al.*, 1997), the Noah land surface model (Chen and Dudhia, 2001) and the Purdue Lin cloud microphysics scheme (Chen and Sun, 2002). In this study, a high-resolution numerical simulation is performed with a horizontal grid interval of 250 m. Thus, a planetary boundary layer parametrization is not applied. Instead, the prognostic turbulent kinetic energy equation for 1.5-order turbulence closure is adopted to calculate horizontal and vertical diffusion coefficients (eddy viscosities). To damp out poorly resolved kinematic features with wavelengths of two to four times the grid interval, the sixth-order spatial filter (Knievel *et al.*, 2007) is used. Note that simulation results (e.g. aspect ratio of convective cells) for a horizontal grid interval of 250 m were similar to those for a horizontal grid interval of 125 m. Hence, a horizontal grid interval of 250 m is chosen in this study. As an urban module, the single-layer urban canopy model (Seoul National University Urban Canopy Model, SNUUCM) recently developed by Ryu *et al.* (2011) is used. The SNUUCM is coupled with the Noah land surface model in a tile approach in the WRF model.

An idealized two-dimensional simulation is performed using the coupled WRF-SNUUCM model under a fair-weather condition. No initial background wind is considered in the simulation. The latitude is set to 30°N. The Coriolis force is excluded. The horizontal domain size is 200 km. The vertical domain size is 6 km, including a 2 km Rayleigh damping layer. There are 65 vertical layers, and the vertical grid interval is stretched with height, starting from 60 m above the surface. The periodic boundary condition is

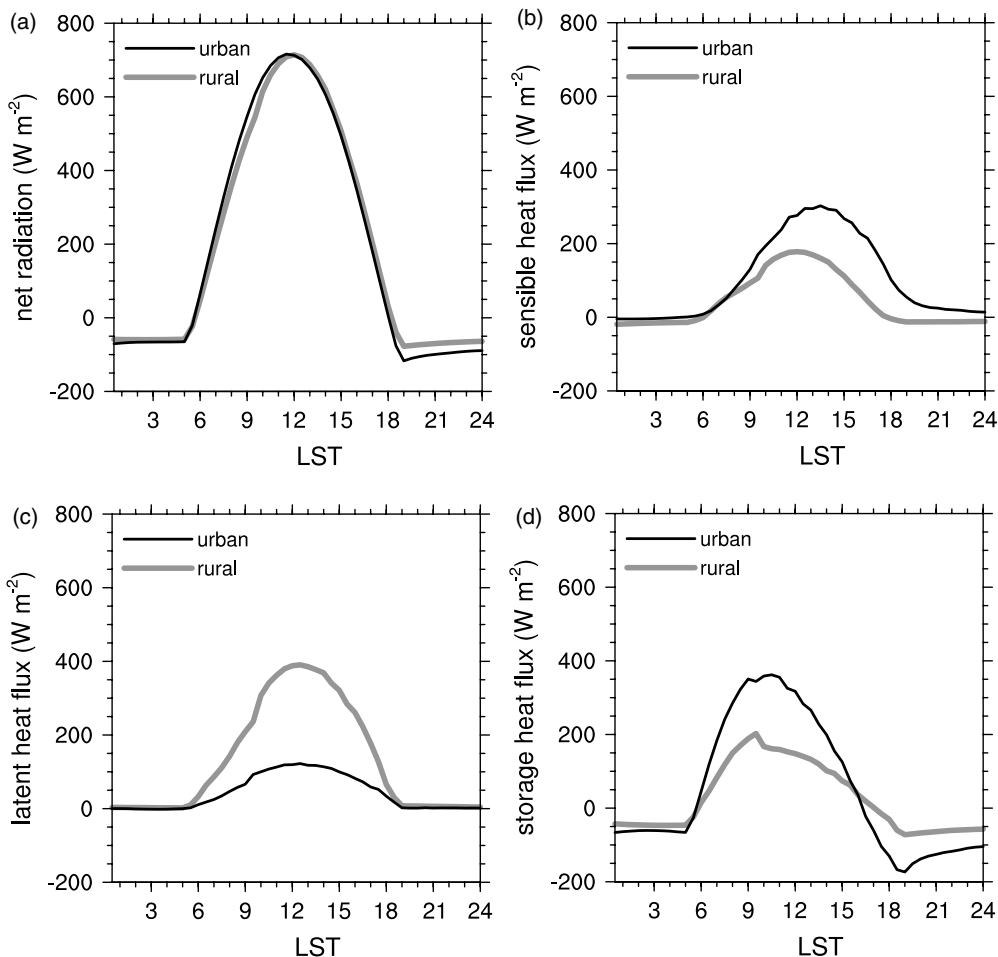


**Figure 1.** Diurnal variation of each component of the surface energy balance averaged over the urban and rural areas. (a) Net radiation, (b) sensible heat flux, (c) latent heat flux and (d) storage heat flux. The urban-area average is taken from  $x = 90$  to  $110$  km, and the rural-area average is taken from  $x = 130$  to  $150$  km.

applied at the lateral boundaries. The lapse rate of the initial potential temperature is  $5\text{ K km}^{-1}$ , and the initial potential temperature near the surface is  $298\text{ K}$ . A relatively dry condition is considered: the initial relative humidity is constant (30%) from the surface to  $z = 4\text{ km}$  and then decreases linearly with increasing height to  $z = 6\text{ km}$  (10%). The simulation starts at 0000 LST 20 June 2008 (the year has no meaning) and is performed for 24 h with a time step of 2 s.

A city with a size of 20 km is considered, and its centre is located at the centre of the model domain. The city is surrounded by a rural area with a cropland–woodland mosaic. The vegetation fraction of the rural area is 0.6, and the soil type is loamy sand. For the four soil layers, the initial soil moisture content (volume of water per volume of soil) and soil temperature are set to 0.25 and  $20^\circ\text{C}$ , respectively. In the urban area, the area fraction of a built-up area is set to 0.8 and the remaining area is set to natural area. The land use/land cover and soil type of the natural area in the urban area are set to the same as those of the rural area. The roof fraction in the built-up area is 0.5. The mean building height is 15 m, and the canyon aspect ratio (height-to-width ratio of the canyon) is 1. All albedos and emissivities of the roof, walls and road are set to 0.2 and 0.95, respectively. Weak anthropogenic heat is included, and its temporal profile is adopted from the profile of the summertime anthropogenic heat estimated in Lee *et al.* (2009): the maximum, minimum

and 24-h average anthropogenic heat fluxes are  $21\text{ W m}^{-2}$  at 1900 LST,  $10\text{ W m}^{-2}$  at 0500 LST and  $16\text{ W m}^{-2}$ , respectively.

### 3. Results and discussion

#### 3.1. Surface energy balance and overall convective boundary layer structure

Figure 1 shows the diurnal variation of each component of the urban and rural SEBs that are averaged over the regions from  $x = 90$  to  $110$  km and from  $x = 130$  to  $150$  km, respectively. In the daytime, the net radiation in the urban area is similar to that in the rural area (Figure 1(a)). Due to the shortwave radiation trapping effect, more shortwave radiation is absorbed in the urban area. However, the amount of emitted longwave radiation is larger in the urban area because of the higher surface temperature in the urban area than in the rural area, especially in the late afternoon. These yield a small difference in the net radiation between the two areas. A similar result was found in the St Louis metropolitan area and surrounding rural area under a clear sky condition in summertime, exhibiting a lower loss of reflected radiation and a greater loss of emitted radiation in the urban area (White *et al.*, 1978).

The difference in the surface features, which are characterized primarily by impervious and pervious surfaces

in urban and rural areas, respectively, is largely responsible for the difference in the SEB and consequently the UHI in the daytime. The differences in sensible heat, latent heat and storage heat fluxes are prominent in the daytime (Figure 1(b)–(d)). In the early morning, due to a significant conversion of the available net radiation into the storage heat flux (Figure 1(d)), the sensible heat flux in the urban area is slightly smaller than that in the rural area. Unlike the urban area, in the rural area, a significant proportion of the available net radiation is converted into the latent heat flux, thus leading to the large difference in latent heat flux between the two areas. In the afternoon, however, the sensible heat flux in the urban area is larger than that in the rural area. The energy fluxes simulated in this study show the well-known characteristics of urban and rural SEBs observed in many cities and their surrounding areas (e.g. Piringer *et al.*, 2007; Hidalgo *et al.*, 2008a).

Due to the larger sensible heat flux in the urban area from late morning, the air temperature in the CBL is higher in the urban area than in the rural area (Figure 2(a)). The temperature excess in the urban area and differential CBL height between the two areas are small in the morning but increase as the differential sensible heat flux increases with time. At  $z = 30$  m, the temperature excess is 0.4 K at 0950 LST and 0.9 K at 1300 LST. The maximum temperature excess in the daytime at  $z = 30$  m appears at 1600 LST with a value of 1.7 K, and the differential CBL height is 520 m at 1600 LST. Because of the small latent heat flux, the water vapour mixing ratio is low in the urban area (Figure 2(b)). At  $z = 30$  m, the water vapour deficit is  $1.51 \text{ g kg}^{-1}$  at 0950 LST,  $1.21 \text{ g kg}^{-1}$  at 1300 LST and  $1.17 \text{ g kg}^{-1}$  at 1600 LST. The temperature excesses and water vapour deficits in the afternoon are similar to those observed in previous studies (Dirks, 1974; Hidalgo *et al.*, 2008a). Interestingly, the water vapour deficit decreases with time. This is due to water vapour transport by the UBC in the afternoon, which is discussed further in the following subsections.

### 3.2. Urban breeze morphology

At 0922 LST, the onset of the UBC is detected by weak inward (outward) flow toward the urban area (the surroundings) in the lower (upper) CBL and by updrafts that correspond to the urban-breeze fronts near the urban–rural boundaries (not shown). Here, the urban-breeze front is defined as the leading edge of the UBC where the maximum vertical velocity appears (see Figure 3). The small and weak circulation at 0922 LST results from the horizontal temperature gradient between the urban and rural areas. As the temperature excess increases with time (Figure 2(a)), the UBC becomes larger and stronger and the two fronts that originate from the urban–rural boundaries move toward the urban centre.

Figure 3 shows an  $x$ – $t$  diagram of vertical velocity at the seventh lowest model level ( $z = 400$  m) and the time series of the maximum vertical velocities and maximum water vapour mixing ratios following the urban-breeze front (hereafter, simply front) and following the two selected cell updrafts (named c1 and c2). In Figure 3, it is shown that a number of convective cells consisting of updrafts and downdrafts form in the rural and urban areas. The cell updrafts in the rural area as well as in the urban area merge with each other around 1400 LST and are then intensified. Accordingly, the cell wavelength between the cell updrafts increases.

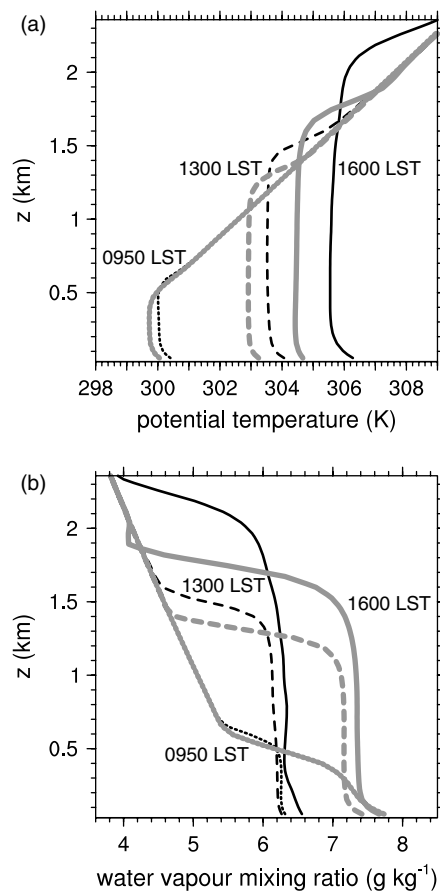


**Figure 2.** Vertical profiles of (a) potential temperature and (b) water vapour mixing ratio averaged over the urban area (thin black lines) and rural area (thick grey lines) at 0950 (dotted lines), 1300 (dashed lines) and 1600 LST (solid lines). The average is taken over the same urban and rural regions as in Figure 1.

Figure 4 shows the fields of horizontal and vertical velocities, potential temperature and water vapour mixing ratio in the developing stage of the UBC at 1600 LST. A larger and stronger UBC is apparent with two strong fronts at  $x = 95.75$  and  $105.5$  km (Figure 4(a) and (b)). The horizontal extent of the UBC is  $\sim 12$  km on each side. At this time, a plume of warm air forms over the urban area and the temperature excess is prominent (Figure 4(c)) in accordance with the large sensible heat flux in the urban area. A number of cell updrafts and downdrafts are also represented in Figure 4(b). Interestingly, some cell updrafts within the UBC (e.g. the cell updraft at  $x = 84.75$  km) have smaller vertical extent and weaker intensity than others outside the UBC. This is because they lose their characteristics to some extent under the influence of the UBC.

As an example, the cell updraft located at  $x = 85.75$  km at 0940 LST (named c1) is traced and its maximum vertical velocity and maximum water vapour mixing ratio are plotted (Figure 3). Before c1 is affected by the UBC (before 1350 LST), its maximum vertical velocity increases and then remains little changed. However, the vertical velocity decreases after the UBC extends to the point where c1 is located and then remains at a low value until 1540 LST. A similar feature is also seen in other cell updrafts when they are under the influence of the UBC. The decrease in vertical velocity in the cell updrafts under the influence of the UBC is similar to that in horizontal convective rolls in the case of a dryline, which is attributed to the descending

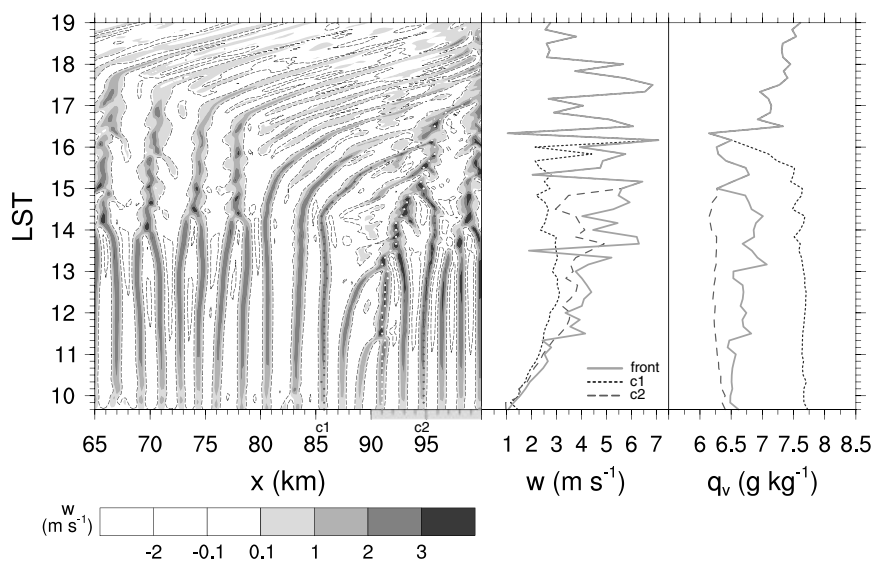


**Figure 3.** Temporal and spatial change of vertical velocity at the seventh lowest model level ( $z = 400$  m) is shown on the left. Only half the urban area (the grey box on the  $x$  axis) is illustrated. The negative contour levels of  $-2.0$  and  $-0.1$  m s $^{-1}$  are represented by dashed lines. The white dots represent the locations of the front, and the black dots represent the locations of the two selected cell updrafts (c1 and c2). The maximum vertical velocities following the front and following c1 and c2 are shown in the middle. The maximum water vapour mixing ratios following the front and following c1 and c2 are shown on the right.

motion of the circulation. According to Xue and Martin (2006), due to suppression by a broad branch of descending motion that is part of the developing mesoscale dryline circulation, horizontal convective rolls often cease to exist or significantly weaken east of the dryline convergence boundary. In addition, the upper part of the UBC becomes slightly stable due to the advection of warm air from the city by the outward flow of the UBC (Figures 4(c) and 5(c)). Thus, the cell updrafts weaken when they are under the influence of the UBC. However, cell updraft c1 is found to be intensified when it is close to the front (Figure 3). Further examination of the cells modified by the UBC is given in section 3.5. Cell updraft c1 is advected by the UBC. The moving speed of c1 is  $1.6$  m s $^{-1}$ , and the horizontal wind speed of the UBC averaged over the depth of the inward flow is  $1.9$  m s $^{-1}$ . Cell updraft c2, an example of the cell updrafts that originate from the urban area, exhibits slightly different behaviour. Cell updraft c2 is characterized by stronger vertical velocity and lower water vapour mixing ratio than c1. The characteristics of the convective cells are discussed in more detail in section 3.4.

As the cell updrafts that originate from both the rural and urban areas interact with the front, the front intensity significantly increases. For example, cell updrafts c1 and c2 largely contribute to the increase in vertical velocity at the front at 1610 and 1510 LST, respectively (Figure 3). After merging with c1 at 1610 LST, the maximum vertical velocity at the front increases by  $3.2$  m s $^{-1}$  between 1600 and 1610 LST (see Figure 9 for more detail). The interaction between the front and convective cells that form in the urban area is similar to that in the case of a sea breeze (e.g. Ogawa *et al.*, 2003). The sea-breeze front interacts with pre-frontal convective cells that form over land ahead of the front and that are little influenced by the sea breeze. In the urban environment, however, the UBC (and, of course, urban-breeze front) also interacts with other types of cells that are modified by the UBC itself.

In Figure 4(d), it is seen that following the inward flow in the lower CBL a considerable amount of water vapour

is brought to the urban area from the rural area with the apparent contrast of water vapour mixing ratio near the fronts. In particular, the relatively large increases in the maximum water vapour mixing ratio at the front are highly related to the merging with the cell updrafts that originate from the rural area, e.g. the increases at 1130, 1310, 1520, 1610 and 1630 LST (Figure 3). For example, the maximum water vapour mixing ratio at the front increases by  $0.53$  g kg $^{-1}$  between 1300 and 1310 LST by merging with the cell updraft that is located at  $x = 87.5$  km at 0940 LST. The increase in the maximum water vapour mixing ratio at the front cannot be explained only by the water vapour transport by the inward flow of the UBC because the transport continues after the UBC develops. However, the maximum water vapour mixing ratio at the front decreases when the front merges with the cell updrafts that originate from the urban area, e.g. at 1340, 1430 and 1500 LST. This is due to the characteristic of drier urban cells. The characteristics of the convective cells and the interaction between the front and the convective cells are further examined in sections 3.4 and 3.5, respectively.

At 1730 LST, the two fronts finally merge with each other at the urban centre. This leads to a strong vertical velocity at the urban centre with  $6.9$  m s $^{-1}$  (Figure 3). In addition, the maximum water vapour mixing ratio increases to  $7.27$  g kg $^{-1}$  at 1730 LST. Figure 5 shows the fields of horizontal and vertical velocities, potential temperature and water vapour mixing ratio at 1730 LST. The horizontal extent of the UBC is  $\sim 60$  km (about three times the size of the city), and this is similar to that documented by Hidalgo *et al.* (2008a). The average intensity of the inward flow of the UBC is  $3.4$  m s $^{-1}$ . It is clearly seen that in the upper part of the CBL the warm air is advected from the city to the surroundings by the outward flow of the UBC. The increase in water vapour mixing ratio over the urban area is more clearly seen as compared with that at 1600 LST, resulting from the water vapour transport by the UBC. After the merging of the two fronts, the vertical velocity at the urban centre decreases with time (Figure 3). The convective

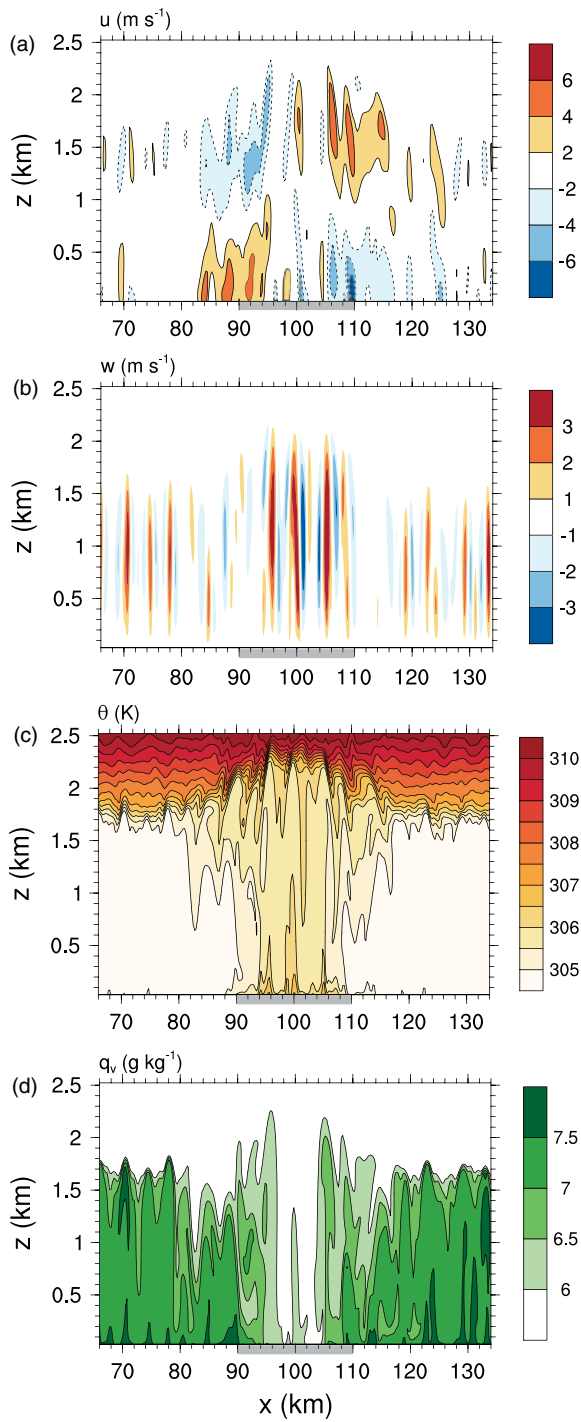


**Figure 4.** Fields of (a) horizontal velocity, (b) vertical velocity, (c) potential temperature and (d) water vapour mixing ratio at 1600 LST. The grey box on the  $x$  axis represents the urban area.

cells become very weak around sunset (1856 LST) because of an absence of surface heating, and they finally disappear in the night-time. Unlike convective cells, however, the UBC still exists even in the night-time but its intensity and size are much reduced under the stable condition (not shown).

### 3.3. Vorticity dynamics of the UBC

To examine the vorticity dynamics of the UBC, a vorticity budget analysis is performed. The  $y$  vorticity equation (Buban *et al.*, 2007) is given in Eq. (1). Note that the Coriolis and turbulence terms are not considered in this

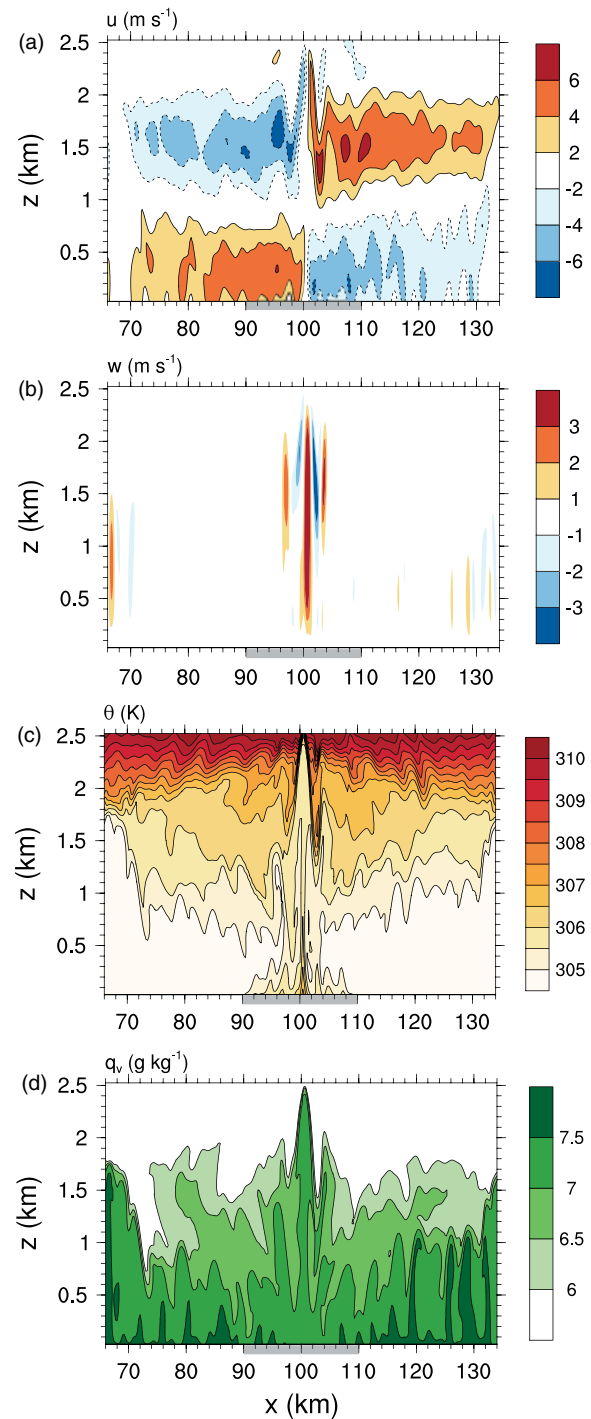


**Figure 5.** Same as in Figure 4 but for 1730 LST.

budget analysis.

$$\begin{aligned} \frac{D\eta}{Dt} = & -\eta \left( \frac{\partial u}{\partial x} + \frac{\partial w}{\partial z} \right) \\ & - c_p \frac{\partial \theta_{v0}}{\partial z} \frac{\partial \pi'}{\partial x} - \frac{g}{\theta_{v0}} \frac{\partial \theta'_v}{\partial x}, \end{aligned} \quad (1)$$

where  $\eta$  is the  $y$  component of vorticity,  $u$  and  $w$  are the components of the wind velocity in the  $x$  and  $z$  directions, respectively,  $c_p$  is the specific heat capacity at constant pressure,  $\theta_{v0}$  is the base-state virtual potential temperature,  $\pi'$  is the perturbation Exner function,  $g$  is the acceleration of gravity and  $\theta'_v$  is the perturbation virtual

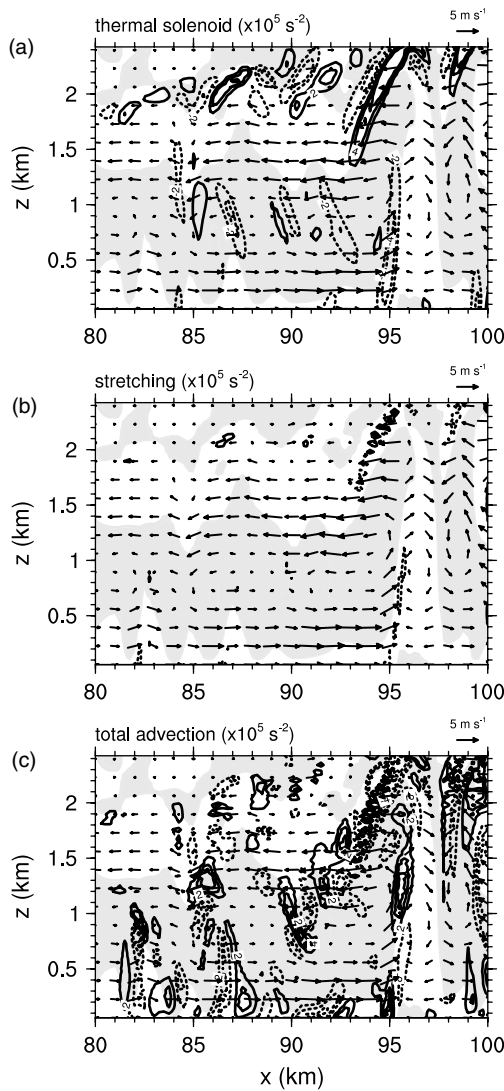


**Figure 6.** Wind fields and the forcing terms of the  $y$  vorticity equation at 1620 LST, (a) thermal solenoid, (b) stretching and (c) total (horizontal and vertical) advection. The region of negative vorticity is shaded. The contour levels are  $-6 \times 10^{-5}$ ,  $-4 \times 10^{-5}$ ,  $-2 \times 10^{-5}$ ,  $2 \times 10^{-5}$ ,  $4 \times 10^{-5}$  and  $6 \times 10^{-5} \text{ s}^{-2}$  for (a) and (c) and  $-3 \times 10^{-5}$ ,  $-2 \times 10^{-5}$ ,  $-1 \times 10^{-5}$ ,  $1 \times 10^{-5}$ ,  $2 \times 10^{-5}$  and  $3 \times 10^{-5} \text{ s}^{-2}$  for (b).

potential temperature. The right-hand side terms (from left to right) are the stretching, perturbation pressure solenoid and thermal solenoid forcing terms.

The thermal solenoid, stretching and total advection (horizontal and vertical advection) terms at 1620 LST are depicted in Figure 6. The pressure solenoid forcing is much weaker than the others by two orders of magnitude, so it is not shown here. The thermal solenoid forcing is strong behind the front, resulting from the strong virtual potential temperature gradient across the front. The sign of the vorticity of the UBC is negative (i.e. counterclockwise rotation), so the negative thermal solenoid forcing acts to enhance the circulation. The negative thermal solenoid forcing continuously contributes to the vorticity of the UBC behind the front from the initial stage of the UBC (not shown). The persistent thermal solenoid forcing is primarily responsible for the generation of the UBC as analogous to other thermally induced circulations such as sea-breeze circulations (e.g. Anthes, 1978) and dryline circulations (e.g. Ziegler *et al.*, 1995; Buban *et al.*, 2007; Wakimoto and Murphrey, 2010). The stretching forcing has a smaller impact

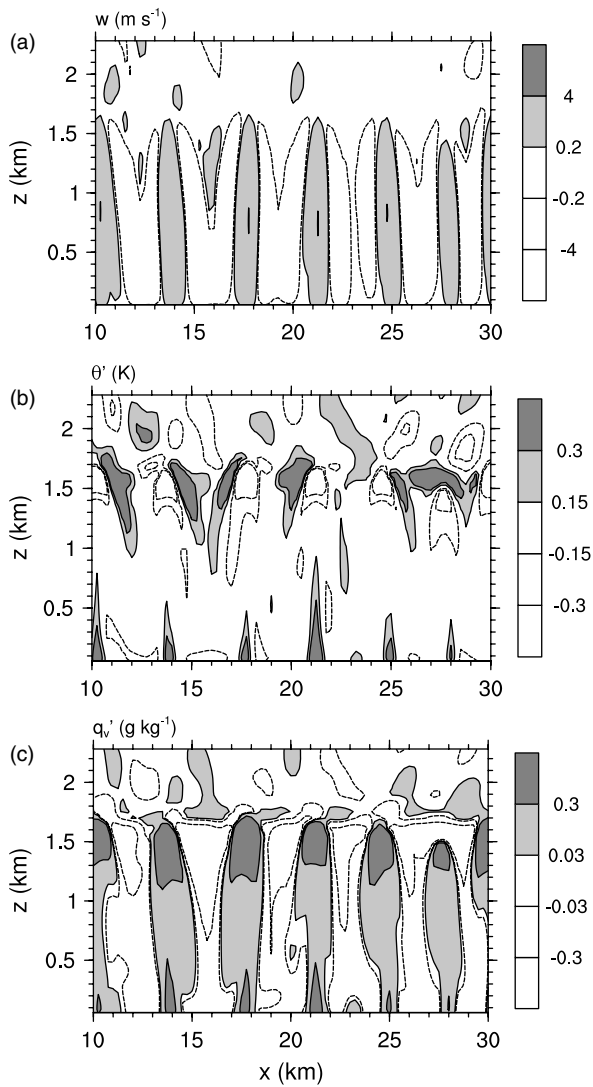
on the UBC than the thermal solenoid forcing by a factor of four (Figure 6(b)). In Figure 6(c), it is clearly seen that the vorticity that results from the cell updrafts and downdrafts in the rural area is advected by the UBC, showing alternating signs. Thus, the cells that originate from the rural area have effects on the vorticity budget locally where the cells are located depending on the sign of the advection term. In summary, it is concluded that the thermal solenoid forcing is the dominant forcing generating the vorticity of the UBC. In addition, the convective cells advected from the rural area locally contribute to the vorticity of the UBC.

### 3.4. Characteristics of convective cells

There are a large number of studies that have investigated horizontal convective rolls or cellular cells (e.g. LeMone, 1973; Atkinson and Zhang, 1996; Weckwerth *et al.*, 1997, 1999; Bennett *et al.*, 2010). Weckwerth *et al.* (1999) stressed that well-defined horizontal convective rolls occur only while the ratio  $-z_i/L$  is less than  $\sim 25$ , where  $z_i$  is the CBL height and  $L$  is the Monin–Obukhov length, and that cellular cells are the dominant convection as  $-z_i/L$  increases. The values of  $-z_i/L$  in the rural and urban areas where the UBC has no influence on the convective cells are large ( $> 80$ ). At this moment, however, it is hard to state conclusively that the convective cells described in this study are cellular cells or horizontal convective rolls because of the two-dimensional experiment conducted in this study.

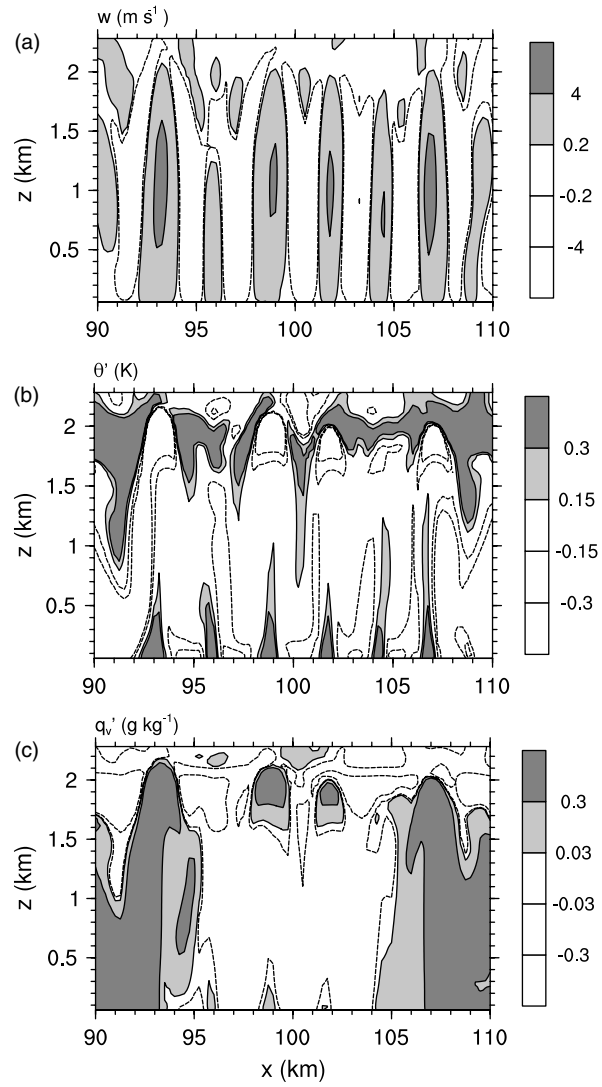
Figure 7 shows the fields of vertical velocity, potential temperature anomaly and water vapour mixing ratio anomaly in the region from  $x = 10$  to 30 km (rural area) at 1430 LST. The anomaly is calculated at each level by subtracting the area-averaged value from the total value. As demonstrated in many previous studies (e.g. Bennett *et al.*, 2010), the cell updrafts are stronger and narrower than the cell downdrafts (Figure 7(a)). The average cell wavelength between the cell updrafts is 3.3 km, and the average aspect ratio (ratio of cell wavelength to cell height) is 2.2. The simulated cell wavelength is similar to that observed over land:  $\sim 3$  km (Weckwerth *et al.*, 1999) and 2–4 km (Bennett *et al.*, 2010). Warmer air than the environment appears in the lower part of the cell updrafts, and cooler air appears in their upper part (Figure 7(b)). Similar features have been observed for thermals (e.g. Lenschow and Stephens, 1980; Miao *et al.*, 2006). The water vapour mixing ratio anomaly well reflects the features of the cell updrafts/downdrafts and shows consistent positive values in the cell updrafts (Figure 7(c)). The high water vapour mixing ratio in the updraft regions is due to the upward transport of moist surface air (Brummer, 1985; Atkins *et al.*, 1995). The entrainment of drier air from the free atmosphere into the downdraft regions is responsible for the large positive water vapour mixing ratio anomaly in the upper part of the cell updrafts. As demonstrated by Miao *et al.* (2006), the positive potential temperature anomaly in the cell updrafts mainly contributes to the buoyancy force (linearly proportional to  $\theta'_v$ ) in the lower CBL and the positive water vapour mixing ratio anomaly contributes to the buoyancy force in the upper CBL in the rural area.

Figure 8 shows the fields of vertical velocity, potential temperature anomaly and water vapour mixing ratio anomaly in the urban area at 1430 LST. The urban breeze fronts are located at  $x = 93$  and 107 km, and these are clearly seen in the potential temperature and water vapour mixing



**Figure 7.** Fields of (a) vertical velocity, (b) potential temperature anomaly and (c) water vapour mixing ratio anomaly in the region from  $x = 10$  to 30 km (rural area) at 1430 LST. The negative contour levels given on the label bars are represented by dashed lines.

ratio anomaly fields (Figure 8(b) and (c)). Here, only the region between the fronts is analysed and the area-average values over this region are used for calculating the potential temperature and water vapour mixing ratio anomalies. The characteristics of the convective cells in the urban area are considerably different from those in the rural area. The cell height (CBL height) in the urban area is, on average, 250 m higher than that in the rural area. The average aspect ratio in the urban area (1.6) is smaller than that in the rural area, and the deeper CBL partly contributes to this. The vertical velocity in the cell updrafts is stronger in the urban area than in the rural area (Figures 7(a) and 8(a)). The positive potential temperature anomaly in the cell updrafts is larger and even extended to a higher level as compared with that in the rural area (Figures 7(b) and 8(b)). The positive water vapour mixing ratio anomaly in the cell updrafts near the surface in the urban area is not as evident as that in the rural area because of the small water vapour supply from the urban surface (i.e. the small latent heat flux). The large water vapour mixing ratio anomaly in the upper part of the cell updrafts, however, is prominent in the urban area, resulting from the entrainment of drier air from the free atmosphere



**Figure 8.** Same as in Figure 7 but for the urban area from  $x = 90$  to 110 km.

into the downdraft regions. The large temperature excess and small moisture excess of the cell updrafts in the urban area imply that the temperature plays a more important role in the buoyancy force in the urban CBL than in the rural CBL, at least in the lower CBL. The different characteristics of the convective cells in the two areas result from the difference in the surface characteristics and consequently the SEB.

### 3.5. Interaction between the UBC and convective cells

To examine the interaction between the front and the convective cells and the impact of the interaction on water vapour mixing ratio in further detail, an example of cell updraft c1 is given in Figure 9. The locations of the front and c1 are represented by the thick and the thin arrows, respectively. Cell updraft c1 located at  $x = 90$  km at 1530 LST merges with a compensating updraft that forms in the vicinity of the downdraft to the left of the front at 1544 LST as c1 is advected by the UBC and then is intensified (Figure 9(c)). As c1 moves toward the front, it encounters the downdraft to the left of the front and then weakens (Figure 9(d)). Cell updraft c1 encounters the front at 1602 LST, and finally the front is intensified due to the merging (Figure 9(e)) as seen in Figure 3. It is clearly seen that the water vapour distribution

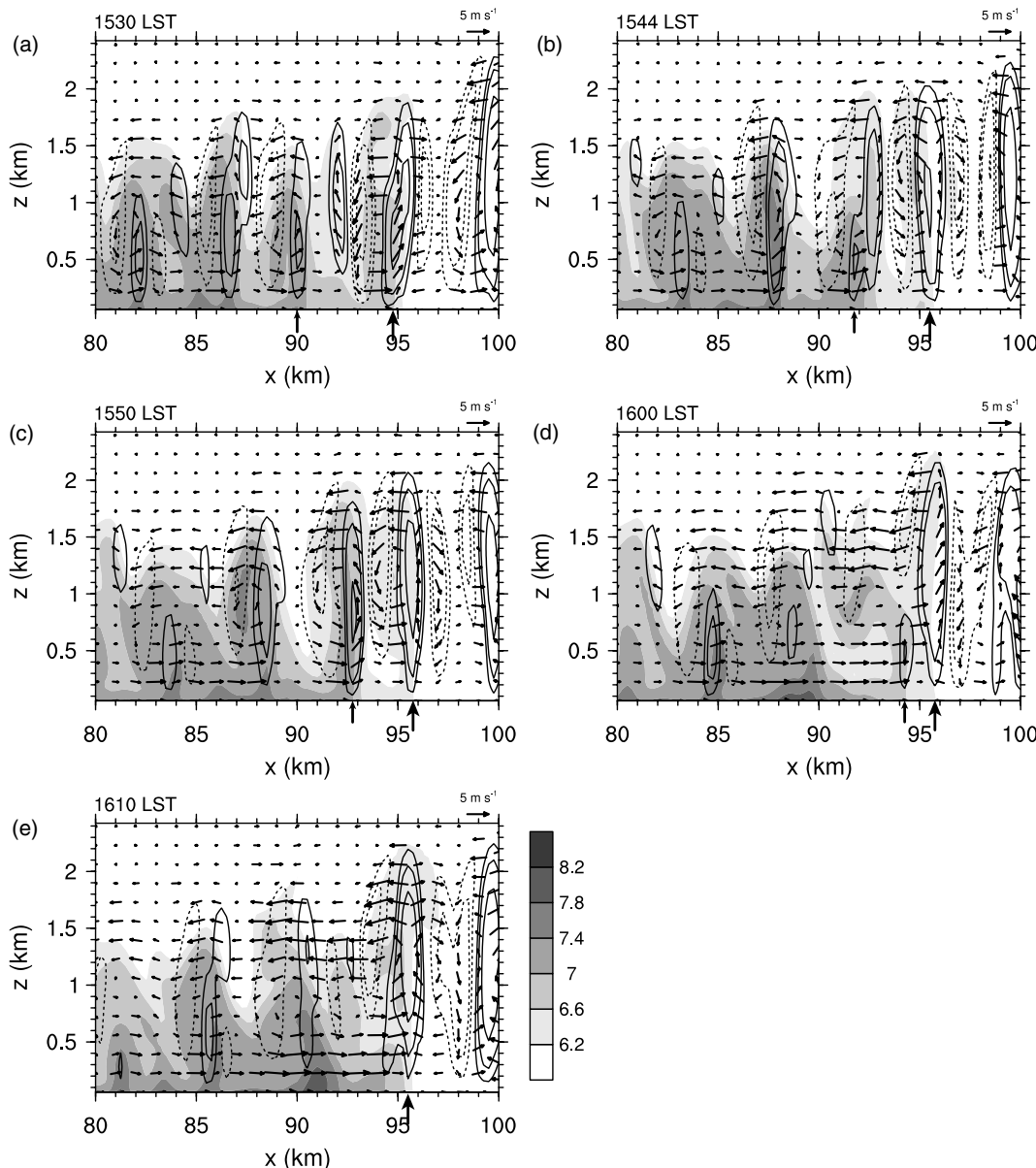


**Figure 9.** Fields of wind, water vapour mixing ratio (shading) and vertical velocity (contours) at (a) 1530, (b) 1544, (c) 1550, (d) 1600 and (e) 1610 LST. The contour levels are  $-4, -2, -1, 1, 2$  and  $4 \text{ m s}^{-1}$ . The negative contour levels are represented by dotted lines. The thick arrows below the  $x$  axis indicate the locations of the front, and the thin arrows the locations of c1.

within the UBC is strongly associated with the convective cells. Initially, the water vapour is concentrated mainly in the cell updrafts in the rural area as seen in Figure 7, but the water vapour in the cell updrafts is dispersed behind the cell updrafts as they are advected by the UBC. Consequently, the cell updrafts act to moisten the atmosphere behind the cell updrafts. The water vapour mixing ratio in the cell updrafts is still high near the surface as long as they are located outside the city. The maximum water vapour mixing ratio in the cell updrafts can therefore remain high as seen in Figure 3, even though the water vapour mixing ratio decreases in the upper part of the cell updrafts. During the merging stage, the water vapour is transported upward within the front (Figure 9(e)), so the water vapour mixing ratio at the front increases as seen in Figure 3. Therefore, the cell updrafts that originate from the rural area act to intensify and moisten the front as they interact with the front.

The merging of the front with the convective cells that form in the urban area is also examined. An example of

cell updraft c2, represented by the thin-dotted arrow, is illustrated in Figure 10. Before c2 interacts with the front, it merges with the downdraft to the right of the front and hence weakens (Figure 10(b)). The front encounters c2 at 1454 LST, and they finally merge with each other at 1510 LST. As a result of the interaction, the front intensity increases by  $1.0 \text{ m s}^{-1}$  between 1450 and 1510 LST. Unlike the merging with the rural cells, the water vapour mixing ratio at the front decreases when the front merges with the cell updrafts that originate from the urban area because the urban cell updrafts are drier than the rural ones as demonstrated in section 3.4 (Figure 8). The increase in front height is larger when the front merges with c2 (by  $\sim 200 \text{ m}$  from 1450 to 1510 LST) than when it merges with c1 (by  $\sim 100 \text{ m}$  from 1550 to 1610 LST).

To examine the three-dimensional nature of a UBC and convective cells, a three-dimensional simulation is performed. The experimental design and preliminary results are given in the appendix.

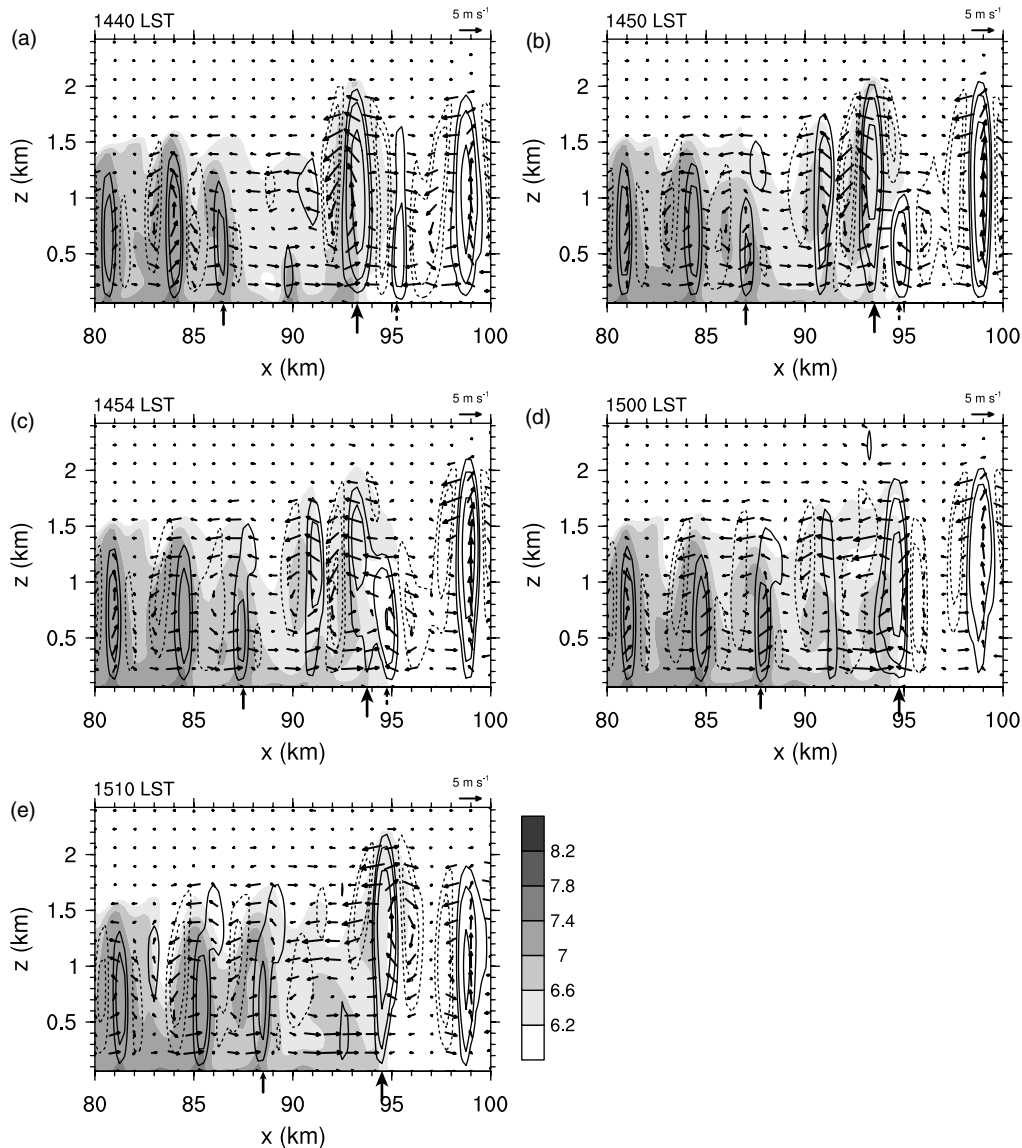


**Figure 10.** Fields of wind, water vapour mixing ratio (shading) and vertical velocity (contours) at (a) 1440, (b) 1450, (c) 1454, (d) 1500 and (e) 1510 LST. The contour levels are  $-4, -2, -1, 1, 2$  and  $4 \text{ m s}^{-1}$ . The negative contour levels are represented by dotted lines. The thick arrows below the  $x$  axis indicate the locations of the front, the thin arrows the locations of  $c1$ , and the thin-dotted arrows the locations of  $c2$ .

#### 4. Summary and conclusions

The structure and evolution of daytime UBC and its interaction with convective cells that form in both the rural and urban areas were examined using the WRF model coupled with the Seoul National University Urban Canopy Model (SNUUCM) under an ideal fair-weather condition. The distinctive urban SEB is well represented, which is predominantly characterized by large sensible heat flux and small latent heat flux in the daytime. As the differential sensible heat flux increases with time, the temperature excess and the CBL height accordingly increase in the urban area. As a result, the UBC that is accompanied by the two strong fronts as the leading edges of the circulation starts to develop in the morning and becomes larger and stronger with time. The water vapour deficit in the urban area is large in the morning but becomes small as a significant amount of water vapour is transported from the rural area by the UBC. By performing a vorticity budget analysis, it was found that the UBC is primarily forced by the thermal solenoid.

Due to the strong surface heating in the daytime, a large number of convective cells form in both the rural and urban areas. In the rural area, the positive (negative) potential temperature anomaly appears in the lower (upper) part of the cell updrafts and the positive water vapour mixing ratio anomaly appears consistently in the cell updrafts. However, different characteristics were found for the urban cells. The aspect ratio of the urban cells is smaller than that of the rural cells, which is partly attributed to the deeper CBL in the urban area. The intensity of the cell updrafts in the urban area is greater than that in the rural area. The positive potential temperature anomaly in the cell updrafts is larger and even extends to a higher level in the urban area. The positive water vapour mixing ratio anomaly in the cell updrafts near the surface in the urban area is not as evident as that seen in the rural area. These different characteristics between the rural and urban cells are attributed to the difference in the SEB between the urban and rural areas.

As the UBC develops, the convective cells that form in the rural area are influenced by the UBC. The cell updrafts weaken and the water vapour mixing ratio in the cell updrafts

decreases when they are advected by the UBC. As the cell updrafts that originate from both the rural and urban areas merge with the front, the front intensity significantly increases. When the front merges with the cell updrafts advected from the rural area, the water vapour mixing ratio at the front increases. When, however, the front merges with the cell updrafts that originate from the urban area, the water vapour mixing ratio at the front decreases. As the UBC develops in the daytime, the two fronts that initially form at the urban–rural boundaries in the morning move toward the urban centre and finally merge with each other in the late afternoon, yielding a strong upward motion at the urban centre.

In this study, the background wind is not considered. The background wind would influence daytime urban breeze circulation and its interaction with convective cells. The degree of the influence would depend largely on the strength of the background wind. This research deserves an investigation.

### Acknowledgements

The authors thank two anonymous reviewers for providing valuable comments on this work. This work was supported by the National Research Foundation of Korea (NRF) grant funded by the Korea Ministry of Education, Science and Technology (MEST) (No. 2012-0005674).

### Appendix

A three-dimensional simulation with a horizontal grid interval of 250 m is performed. A circular shaped-city with a diameter of 20 km is considered, and its centre is located at the centre of the model domain. The horizontal domain size is 120 km × 120 km, and the time step is 0.5 s. The other experimental set-up and physical parametrization options are the same as those used in the two-dimensional simulation.

The time evolutions of a UBC and of convective cells that originate from the rural and urban areas are depicted in Figure A1. It is seen that the urban-breeze fronts interact with the convective cells originating from both the rural and urban areas as the fronts move toward the urban centre. This interaction leads to the strong upward motions at the intersection points, similar to that seen in the two-dimensional simulation.

It is also revealed that the UBC and convective cells have three-dimensional characteristics. Figure A2 shows the horizontal wind and vertical velocity fields at  $z = 400$  m and at 1400 LST. Cellular type convection forms in both the rural and urban areas, and due to the shape of the city the urban-breeze front has a circular shape. The inward flow toward the urban area as a part of the UBC forms in the lower boundary layer (Figure A2) and becomes stronger with time (not shown). An interesting feature is found in the three-dimensional simulation: under the influence of the UBC, the convective cells originating from the rural area are deformed from a cellular type to a roll-like type. This deformation is probably attributed to the inward flow of the UBC.

Based on preliminary analyses, it is noticed that there are some similarities between the two- and three-dimensional simulations. The interaction between the urban-breeze front and convective cells is also found in the three-dimensional simulation. The different characteristics of convective cells between urban and rural cells shown in Figures 7 and 8 are also identified in the three-dimensional simulation (not shown). That is, the urban cell updrafts are stronger, warmer and drier than rural ones. However, the nature of phenomena simulated in two and three dimensions is essentially different, e.g. the deformation of convective cells in the three-dimensional simulation. Further in-depth analyses are required and will be made to explore the three-dimensional characteristics of convective cells and the interaction between a UBC and convective cells. Analysis results will be reported in a separate article.

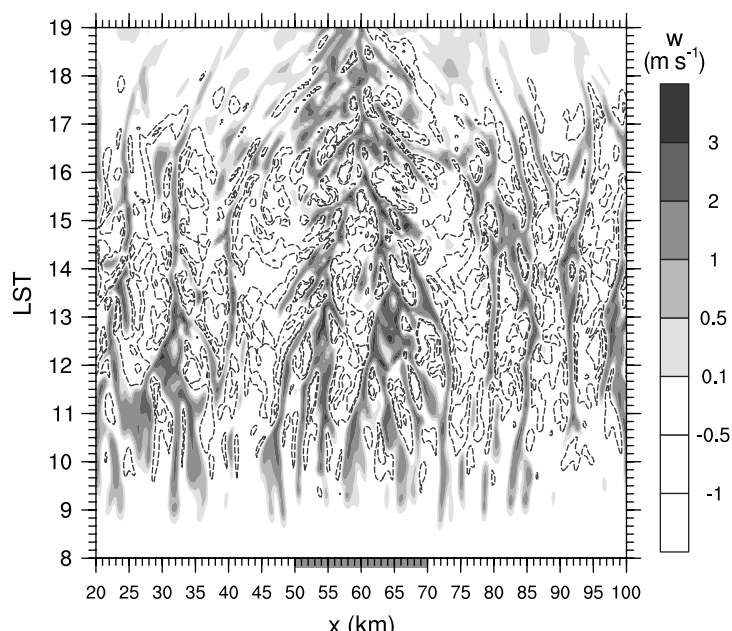


**Figure A1.** Temporal and spatial change of vertical velocity at the seventh lowest model level ( $z = 400$  m) and at  $y = 60$  km in the three-dimensional simulation. The urban area is represented by the grey box on the  $x$  axis. The negative contour levels of  $-1.0$  and  $-0.5 \text{ m s}^{-1}$  are represented by dashed lines.

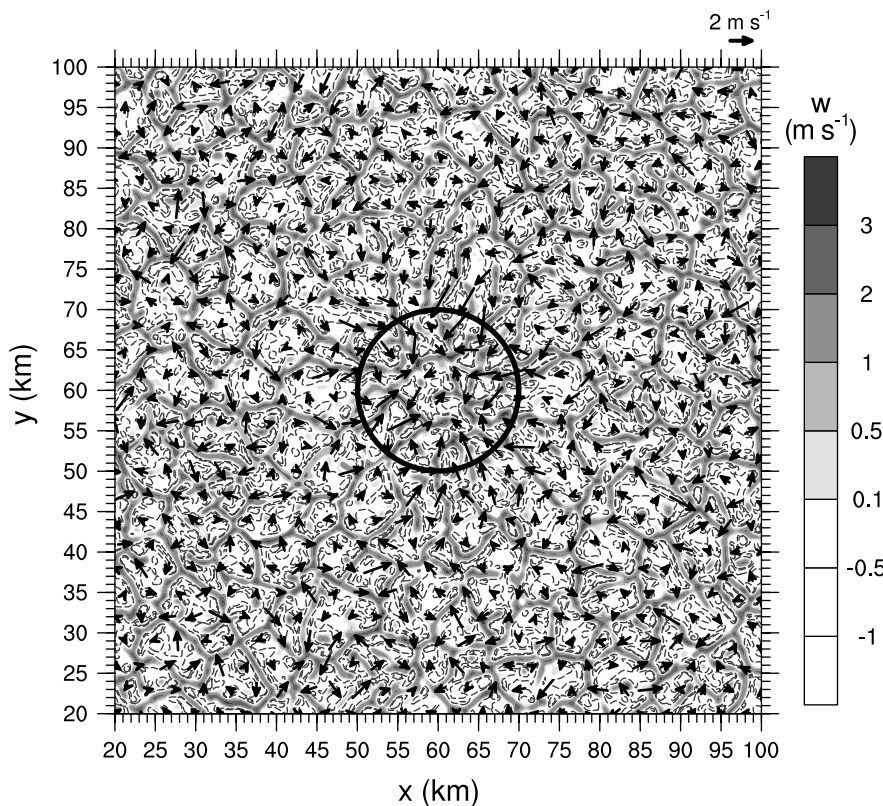


**Figure A2.** Fields of horizontal wind vector and vertical velocity at the seventh lowest model level ( $z = 400$  m) and at 1400 LST in the three-dimensional simulation. The circle indicates the city boundary. The negative vertical velocity contour levels of  $-1.0$  and  $-0.5 \text{ m s}^{-1}$  are represented by dashed lines.

## References

- Anthes RA. 1978. The height of the planetary boundary layer and the production of circulation in a sea breeze model. *J. Atmos. Sci.* **35**: 1231–1239.
- Atkins NT, Wakimoto RM, Weckwerth TM. 1995. Observations of the sea-breeze front during CaPE. Part II: Dual-Doppler and aircraft analysis. *Mon. Weather Rev.* **123**: 944–969.
- Atkins NT, Wakimoto RM, Ziegler CL. 1998. Observations of the finescale structure of a dryline during VORTEX 95. *Mon. Weather Rev.* **126**: 525–550.
- Atkinson BW, Zhang JW. 1996. Mesoscale shallow convection in the atmosphere. *Rev. Geophys.* **34**: 403–431.
- Avissar R. 1996. Potential effects of vegetation on the urban thermal environment. *Atmos. Environ.* **30**: 437–448.
- Baik J-J. 1992. Response of a stably stratified atmosphere to low-level heating – An application to the heat island problem. *J. Appl. Meteorol.* **31**: 291–303.
- Baik J-J, Chun H-Y. 1997. A dynamical model for urban heat islands. *Boundary-Layer Meteorol.* **83**: 463–477.
- Baik J-J, Kim Y-H, Chun H-Y. 2001. Dry and moist convection forced by an urban heat island. *J. Appl. Meteorol.* **40**: 1462–1475.
- Bennett LJ, Weckwerth TM, Blyth AM, Geerts B, Miao Q, Richardson YP. 2010. Observations of the evolution of the nocturnal and convective boundary layers and the structure of open-celled convection on 14 June 2002. *Mon. Weather Rev.* **138**: 2589–2607.
- Brummer B. 1985. Structure, dynamics and energetics of boundary layer rolls from KonTur aircraft observations. *Beitr. Phys. Atmos.* **58**: 237–254.
- Buban MS, Ziegler CL, Rasmussen EN, Richardson YP. 2007. The dryline on 22 May 2002 during IHOP: Ground-radar and in situ data analyses of the dryline and boundary layer evolution. *Mon. Weather Rev.* **135**: 2473–2505.
- Chen F, Dudhia J. 2001. Coupling an advanced land surface–hydrology model with the Penn State–NCAR MM5 modeling system. Part I: Model implementation and sensitivity. *Mon. Weather Rev.* **129**: 569–585.
- Chen S-H, Sun W-Y. 2002. A one-dimensional time dependent cloud model. *J. Meteorol. Soc. Japan* **80**: 99–118.
- Dailey PS, Fovell RG. 1999. Numerical simulation of the interaction between the sea-breeze front and horizontal convective rolls. Part I: Offshore ambient flow. *Mon. Weather Rev.* **127**: 858–878.
- Delage Y, Taylor PA. 1970. Numerical studies of heat island circulations. *Boundary-Layer Meteorol.* **1**: 201–226.
- Dirks RA. 1974. Urban atmosphere: Warm dry envelope over St. Louis. *J. Geophys. Res.* **79**: 3473–3475.
- Dudhia J. 1989. Numerical study of convection observed during the winter monsoon experiment using a mesoscale two-dimensional model. *J. Atmos. Sci.* **46**: 3077–3107.
- Giridharan R, Lau SSY, Ganesh S, Givoni B. 2007. Urban design factors influencing heat island intensity in high-rise high-density environments of Hong Kong. *Build. Environ.* **42**: 3669–3684.
- Hidalgo J, Pigeon G, Masson V. 2008a. Urban-breeze circulation during the CAPITOUL experiment: Observational data analysis approach. *Meteorol. Atmos. Phys.* **102**: 223–241.
- Hidalgo J, Masson V, Pigeon G. 2008b. Urban-breeze circulation during the CAPITOUL experiment: Numerical simulations. *Meteorol. Atmos. Phys.* **102**: 243–262.
- Hidalgo J, Masson V, Gimeno L. 2010. Scaling the daytime urban heat island and urban-breeze circulation. *J. Appl. Meteorol. Clim.* **49**: 889–901.
- Kim Y-H, Baik J-J. 2002. Maximum urban heat island intensity in Seoul. *J. Appl. Meteorol.* **41**: 651–659.
- Knievel JC, Bryan GH, Hacker JP. 2007. Explicit numerical diffusion in the WRF model. *Mon. Weather Rev.* **135**: 3808–3824.
- Kusaka H, Kimura F. 2004. Coupling a single-layer urban canopy model with a simple atmospheric model: Impact on urban heat island simulation for an idealized case. *J. Meteorol. Soc. Japan* **82**: 67–80.
- Lee S-H, Song C-K, Baik J-J, Park S-U. 2009. Estimation of anthropogenic heat emission in the Gyeong-In region of Korea. *Theor. Appl. Climatol.* **96**: 291–303.
- LeMone MA. 1973. The structure and dynamics of horizontal roll vortices in the planetary boundary layer. *J. Atmos. Sci.* **30**: 1077–1091.
- Lemonsu A, Masson V. 2002. Simulation of a summer urban breeze over Paris. *Boundary-Layer Meteorol.* **104**: 463–490.
- Lenschow DH, Stephens PL. 1980. The role of thermals in the convective boundary layer. *Boundary-Layer Meteorol.* **19**: 509–532.
- Lu J, Arya SP, Snyder WH, Lawson RE. 1997a. A laboratory study of the urban heat island in a calm and stably stratified environment. Part I: Temperature field. *J. Appl. Meteorol.* **36**: 1377–1391.
- Lu J, Arya SP, Snyder WH, Lawson RE. 1997b. A laboratory study of the urban heat island in a calm and stably stratified environment. Part II: Velocity field. *J. Appl. Meteorol.* **36**: 1392–1402.

- Miao Q, Geerts B, LeMone M. 2006. Vertical velocity and buoyancy characteristics of coherent echo plumes in the convective boundary layer, detected by a profiling airborne radar. *J. Appl. Meteorol. Clim.* **45**: 838–855.
- Miao S, Chen F, LeMone MA, Tewari M, Li Q, Wang Y. 2009. An observational and modeling study of characteristics of urban heat island and boundary layer structures in Beijing. *J. Appl. Meteorol. Clim.* **48**: 484–501.
- Mlawer EJ, Taubman SJ, Brown PD, Iacono MJ, Clough SA. 1997. Radiative transfer for inhomogeneous atmospheres: RRTM, a validated correlated-k model for the longwave. *J. Geophys. Res.* **102**: 16663–16682.
- Noto K. 1996. Dependence of heat island phenomena on stable stratification and heat quantity in a calm environment. *Atmos. Environ.* **30**: 475–485.
- Ogawa S, Sha W, Iwasaki T, Wang Z. 2003. A numerical study on the interaction of a sea-breeze front with convective cells in the daytime boundary layer. *J. Meteorol. Soc. Japan* **81**: 635–651.
- Oke TR. 1982. The energetic basis of the urban heat island. *Q. J. R. Meteorol. Soc.* **108**: 1–24.
- Oke TR. 1988. The urban energy balance. *Progr. Phys. Geogr.* **12**: 471–508.
- Peckham SE, Wilhelmson RB, Wicker LJ, Ziegler CL. 2004. Numerical simulation of the interaction between the dryline and horizontal convective rolls. *Mon. Weather Rev.* **132**: 1792–1812.
- Piringer M, Joffre S, Baklanov A, Christen A, Deserti M, De Ridder K, Emeis S, Mestayer P, Tombrou M, Middleton D, Baumann-Stanzer K, Dandou A, Karpinen A, Burzynski J. 2007. The surface energy balance and the mixing height in urban areas – activities and recommendations of COST-Action 715. *Boundary-Layer Meteorol.* **124**: 3–24.
- Rao PA, Fuelberg HE, Droegelemeier KK. 1999. High-resolution modeling of the Cape Canaveral area land–water circulations and associated features. *Mon. Weather Rev.* **127**: 1808–1821.
- Ryu Y-H, Baik J-J, Lee S-H. 2011. A new single-layer urban canopy model for use in mesoscale atmospheric models. *J. Appl. Meteorol. Clim.* **50**: 1773–1794.
- Shreffler JH. 1978. Detection of centripetal heat-island circulations from tower data in St. Louis. *Boundary-Layer Meteorol.* **15**: 229–242.
- Skamarock WC, Klemp JB, Dudhia J, Gill DO, Barker DM, Duda MG, Huang X-Y, Wang W, Powers JG. 2008. *A Description of the Advanced Research WRF Version 3*. Technical Note NCAR/TN-475+STR, National Center for Atmospheric Research: Boulder, CO.
- Tian W, Parker DJ, Kilburn CAD. 2003. Observations and numerical simulation of atmospheric cellular convection over mesoscale topography. *Mon. Weather Rev.* **131**: 222–235.
- Vukovich FM. 1971. Theoretical analysis of the effect of mean wind and stability on a heat island circulation characteristic of an urban complex. *Mon. Weather Rev.* **99**: 919–926.
- Wakimoto RM, Murphrey HV. 2010. Analysis of convergence boundaries observed during IHOP\_2002. *Mon. Weather Rev.* **138**: 2737–2760.
- Wakimoto RM, Murphrey HV, Browell EV, Ismail S. 2006. The “triple point” on 24 May 2002 during IHOP. Part I: Airborne Doppler and LASE analyses of the frontal boundaries and convection initiation. *Mon. Weather Rev.* **134**: 231–250.
- Weckwerth TM, Wilson JW, Wakimoto RM, Crook NA. 1997. Horizontal convective rolls: Determining the environmental conditions supporting their existence and characteristics. *Mon. Weather Rev.* **125**: 505–526.
- Weckwerth TM, Horst TW, Wilson JW. 1999. An observational study of the evolution of horizontal convective rolls. *Mon. Weather Rev.* **127**: 2160–2179.
- White JM, Eaton FD, Auer AH. 1978. The net radiation budget of the St. Louis metropolitan area. *J. Appl. Meteorol.* **17**: 593–599.
- Wong KK, Dirks RA. 1978. Mesoscale perturbations on airflow in the urban mixing layer. *J. Appl. Meteorol.* **17**: 677–688.
- Xue M, Martin WJ. 2006. A high-resolution modeling study of the 24 May 2002 dryline case during IHOP. Part II: Horizontal convective rolls and convective initiation. *Mon. Weather Rev.* **134**: 172–191.
- Ziegler CL, Martin WJ, Pielke RA, Walko RL. 1995. A modeling study of the dryline. *J. Atmos. Sci.* **52**: 263–285.